A long-term follow up of 174P/Echeclus

P. Rousselot, P. P. Korsun, I. Kulyk, A. Guilbert-Lepoutre, J.-M. Petit

Monthly Notices of the ROYAL ASTRONOMICAL SOCIETY

MNRAS **462,** S432–S442 (2016) doi:10.1093/mnras/stw3054
Advance Access publication 2016 November 29

A long-term follow up of 174P/Echeclus

P. Rousselot,[1]★ P. P. Korsun,[2] I. Kulyk,[2] A. Guilbert-Lepoutre[1] and J.-M. Petit[1]

[1]*Institut UTINAM UMR 6213, CNRS, Univ. Bourgogne Franche-Comté, OSU THETA, BP 1615, 25010 Besançon Cedex, France*
[2]*Main Astronomical Observatory of NAS of Ukraine, 27 Akademika Zabolotnoho Street, 03680 Kyiv, Ukraine*

Accepted 2016 November 22. Received 2016 November 22; in original form 2016 June 30

ABSTRACT

Centaur 174P/Echeclus, initially designated as (60558) 2000 EC_{98}, presented three outbursts. A first and main one detected in 2005 December, another smaller one detected in 2011 May and a last one at the end of 2016 August. The first outburst was the largest one ever detected for a Centaur, of the order of 30 times that seen in other similar bodies. Because of the special interest of this target, and its brightness, we now have a large set of observational data were obtained before, during and after the two first outbursts. We present here new observational data obtained after the main outburst or coming from archives and an analysis of them. The main results of our study are (i) an absence of light curve in our 2013 data (while it was ∼0.24 mag in the *R*-band in 2002–2003) and (ii) a satisfactory fit of the main outburst with two short events and a longer one (three sources of dust). Both results suggest a high obliquity of the rotation axis. We also discuss the origin of these outbursts and conclude that they are probably related to internal inhomogeneities of the nucleus.

Key words: Comets: general – comets: individual: 174P/Echeclus.

1 INTRODUCTION

Centaurs, which can be defined as small bodies that have their perihelion outside of Jupiter's orbit (5.2 au) and semimajor axis inside of Neptune (30.0 au; Gladman, Marsden & Vanlaerhoven 2008), have unstable orbits. They represent probably an intermediate stage in the process that dynamically transforms a Kuiper belt object (KBO) to a short-period comet (Horner, Evans & Bailey 2004). When a Centaur is active, thus allowing for the study of processes responsible for the physico-chemical alteration of icy bodies, a close look at this object is therefore key for understanding the genetic link between KBOs and comets. The fraction of Centaurs for which a cometary activity has been detected, compared to the whole population of Centaurs, is about 13 per cent (Jewitt 2009).

The first Centaur known to present cometary activity was Chiron. Kowal, Liller & Chaisson (1977) discovered this object and initially classified it as an asteroid. Tholen et al. (1988) suggested, on the basis of non-asteroidal brightness variations, that some kind of cometary activity could occur on this object. Meech & Belton (1989) were the first authors to present a direct detection of Chiron's coma. This object has a semimajor axis $a = 13.67$ au and a perihelion distance $q = 8.45$ au. It is considered a transition object between TNOs and Jupiter family comets.

Since the discovery of cometary activity for Chiron, about 20 Centaurs have now been known to present a cometary activity. Among these objects, the more surprising outburst was observed on the Centaur 174P/Echeclus. It was discovered by the Spacewatch program on 2000 March 3 (Marsden 2000) and initially labelled (60558) 2000 EC_{98}. Table 1 presents the orbital elements of this Centaur. It has an unstable orbit with a lifetime of the order of 10^5 years, well below the typical dynamical lifetime of most of the Centaurs, which is of the order of 10^7 years (Gladman, private communication). Different observers published observational data (mostly photometric) related to this target. They also searched for cometary activity without any success despite a very sensitive search of up to magnitude 27 arcsec^{-2} (Rousselot et al. 2005; Lorin & Rousselot 2007).

On 2005 December 30, a surprising cometary outburst was discovered with the 5-m Mount Palomar Observatory telescope (Choi, Weissmann & Polishook 2006b). This outburst corresponded to a change in the overall visual magnitude from about 21 to about 14. At that time (60558) 2000 EC_{98} was located at 13.07 au from the Sun and was subsequently renamed with a cometary designation: 174P/Echeclus. Subsequent observations revealed that the coma did not appear to be directly associated with the nucleus (Choi et al. 2006a; Weissman et al. 2006; Bauer et al. 2008; Rousselot 2008).

This main outburst lasted a few months and observations performed in 2007 with the 3.5 m New Technology Telescope did not allow us to detect any cometary activity (Rousselot 2008). Another outburst was detected at the end of 2011 May (Jaeger et al. 2011) and lasted a few weeks but was less important than the first one (overall *V* magnitude varying from about 19 to about 14). In addition, this object passed its perihelion on 2015 April 21, at which time it did not show any sign of cometary activity. It is only at the

★ E-mail: phil@obs-besancon.fr

Table 1. Orbital characteristics of Echeclus (from the JPL Small-Body Database, see: http://ssd.jpl.nasa.gov/sbdb.cgi#top). The last time of perihelion passage was 2015 April 21.

a (au)	e	q (au)	Q (au)	i	Period (yr)
10.68	0.455	5.81	15.54	4.°34	34.90

end of 2016 August that a last outburst was observed. This outburst increased the overall brightness by about 2.6 mag and lasted a few weeks.[1]

Since the first photometric observations performed on this object at the very beginning of the 2000s, many observations have now been collected, both when it was active and inactive. This large sample of data allows a long-term study of this peculiar object that covers nearly half of its orbital period from aphelion to perihelion. This paper presents the observational data collected on this target during this period – mostly in photometric mode and in the optical range – and an analysis of the outbursts mechanisms, and the apparent changes in the light-curve.

In Section 2, the observational data are described. Section 3 presents the data analysis. Sections 4 and 5 present a modelling of, respectively, the light-curve changes and the outbursts, and Section 6 presents a discussion related to the long-term behaviour of Echeclus. Section 7 concludes this paper.

2 OBSERVATIONAL DATA

Different sets of observational data have been used for this work. Some of them correspond to data already analysed and published (Rousselot et al. 2005; Rousselot 2008) and some other to new observational data. One set of data comes from archives (see below). The new observational data have been obtained with two telescopes located at La Palma (Spain): the 2.5-m Nordic Optical Telescope (NOT) and the 2-m robotic Liverpool Telescope (LT).

The NOT images were obtained with the Andalucia Faint Object Spectrograph and Camera (ALFOSC) used in imaging mode. In this mode, the field of view is 6.4 arcmin × 64 arcmin using a 2048 × 2048 CCD detector with a 13.5-μm pixel size, corresponding to 0.19 arcsec on the sky. We conducted the observations with broad-band *BVRI* filters, and we also observed a field with standard stars at different airmasses to provide information for the photometric reduction. These images were preprocessed using a bias and a master sky flat-field obtained during the observing run. The photometric coefficients were computed for each photometric observing night thanks to the standard stars images. These photometric coefficients permitted us to compute the magnitudes of different stars appearing in the same field of view (for the observational data obtained in 2013 the different fields of view corresponding to the position of Echeclus during different nights were observed during each photometric night). By performing relative photometry with these stars, considered as reference stars, it was possible to compute the apparent magnitude of Echeclus. For the images obtained in 2011, the photometric coefficients permitted us to compute the cometary activity, expressed as $Af\rho$ values (see Section 3).

The observational data of the 2-m robotic LT were obtained with the optical imaging component of the IO (infrared–optical) suite of instruments (IO:O)and with broad-band Bessell *B*, Bessell *V* and SDSS *R* filters. A field of standard stars (Mark A) was also observed at a similar airmass to provide zero-point photometric coefficients (Landolt 1992). For each of the three different nights of observations, all the images were obtained with short exposure time (30 s) to avoid any problem of trailing effect due to the fast motion of the object. A total of 15 images were obtained with the SDSS *R*, and 8 for both the Bessell *B* and *V* filters. All these observations were performed in robotic mode. We used the preprocessed data provided by the reduction pipeline to analyse these observations.

The archive data come from the 3.6-m Canada–France–Hawaii Telescope (CFHT). They were obtained with the Megacam instrument, a wide field imager equipped with a mosaic of 36 CCDs, that covers a field of view of 1 deg^2 on the sky. Three different images of 60 s exposure each were obtained with an r' filter. The interest of these images is that they were obtained before the official discovery of the main outburst, so they are the first images obtained after this outburst. We used the preprocessed images computed by the reduction pipeline. Photometric calibration of the images to the absolute scale was performed with the photometric coefficients (zero-point, main extinction coefficient and colour term) stored in the header of the image files.

The main technical parameters of the telescopes and CCD detectors are presented in Table 2 and the observing circumstances are summarized in Table 3.

3 DATA PROCESSING

Besides the archive CFHT images, the NOT data obtained in 2011, when Echeclus was active, clearly show the presence of a coma around the nucleus (Fig. 1). These data were used for computing $Af\rho$ parameters. This parameter was introduced by A'Hearn et al. (1984) and permits us to quantify the cometary activity in a manner not too sensitive to the parameters used to quantify dust production rate (e.g. albedo or dust grain density). It corresponds to the product of the bond albedo A, the filling factor f of grains within the field of view and the projected cometocentric distance ρ. This parameter is expressed in centimetres and, in a steady-state coma having a $1/\rho$ variation of the number of dust particles along the line of sight, is supposed to be, more or less independent of the aperture size used to compute it.

However, the majority of the comets observed at large heliocentric distances have indeed surface-brightness profiles (SBPs), which fall down steeper than a canonical $1/\rho$ decrease. It is explained by action of the radiation pressure accelerating dust particles as well as possible sublimation from particles themselves, when they are moving outwards (Jewitt & Meech 1987; Lowry & Fitzsimmons 2005). In order to investigate Echeclus' brightness profile, average images were constructed for each night: one for the target and one for a reference star chosen to have a good signal-to-noise ratio (SNR) and no other star too close to it. In both cases, we shifted the individual images in such a way to put the target/star in the centre, and then the individual images in each group were stacked together. The median filtration was applied to remove faint background stars and possible artefacts. Close bright stars were masked with the neighbour background signal. The SBPs of appropriate background stars were built, calibrated and scaled to the brightness of the target (see Fig. 1). Aperture photometry was performed on the average images to measure total apparent magnitudes of Echeclus and to construct the SBP. For each observing period, the instrumental magnitudes were measured through a series of apertures of monotonically increasing radii from target's optocentre to just beyond the point, where the signal from the coma became comparable to the

[1] This outburst was detected by amateur astronomers (see, e.g. http://lists.britastro.org/pipermail/comets-disc/2016-August/date.html) and started on 2016 August 28.2 ± 0.4.

Table 2. Equipment of the observations (for the observational data corresponding to images). NOT: Nordic Optical Telescope (La Palma). LT: Liverpool Telescope (La Palma). CFHT: Canada–France–Hawaii Telescope. VLT: Very large Telescope (ESO). NTT: New Technology Telescope (ESO). Danish: Danish Telescope (ESO). T 3.6-m: 3.6-m telescope (ESO).

Telescope	Diameter (m)	Instrument	CCD	Scale (arcsec pixel^{-2})	Field of view (arcmin × arcmin)	Filter
CFHT	3.6	Megacam	36 × 2048 × 4612	0.187	60 × 60	r'
NTT	3.58	SUSI 2	2 × 2048 × 4096	0.0805 (binned 2 × 2)	5.5 × 5.5	*B*, *V*, *R*
3.6-m	3.57	EFOSC2	2048 × 2048	0.157 (binned 2 × 2)	5.4 × 5.4	*B*, *V*, *R*
Danish	1.54	DFOSC	2048 × 4096	0.39	13.7 × 13.7	*B*, *V*, *R*
VLT	8.2	FORS 1	2048 × 2048	0.2	6.8 × 6.8	*B*, *V*, *R*
NOT	2.5	ALFOSC	2048 × 2048	0.19	6.5 × 6.5	*B*, *V*, *R*, *I*
LT	2.0	IO:O	4096 × 4112	0.15 (binned 2 × 2)	10 × 10	*B*, *V*, r'

Table 3. Observing circumstances (by chronological order of the observations). *r*: heliocentric distance (au); Δ: geocentric distance (au); α: phase angle.

UT Date	*r*	Δ	α	Data type	Filter/spectral range	Telescope	Comment
2001 Apr. 26	15.16	14.46	2.°8	Image	*B*, *V*, *R*	NTT	See Rousselot et al. (2005)
2001 Apr. 27	15.16	14.47	2.°9	Image	*B*, *V*, *R*	NTT	See Rousselot et al. (2005)
2002 Mar. 18	14.90	13.90	0.°1	Image	*B*, *V*, *R*	Danish	See Rousselot et al. (2005)
2002 Mar. 19	14.90	13.90	0.°2	Image	*B*, *V*, *R*	Danish	See Rousselot et al. (2005)
2002 Mar. 23	14.89	13.90	0.°4	Image	*B*, *V*, *R*	Danish	See Rousselot et al. (2005)
2002 Mar. 24	14.89	13.90	0.°5	Image	*B*, *V*, *R*	Danish	See Rousselot et al. (2005)
2003 Apr. 10	14.50	13.55	1.°4	Image	*B*, *V*, *R*	T 3.6-m	See Rousselot et al. (2005)
2003 Apr. 11	14.49	13.56	1.°4	Image	*B*, *V*, *R*	T 3.6-m	See Rousselot et al. (2005)
2003 Apr. 12	14.49	13.56	1.°5	Image	*B*, *V*, *R*	T 3.6-m	See Rousselot et al. (2005)
2005 Dec. 22	13.08	13.38	4.°1	Image	r'	CFHT	Active. Archive data
2006 Mar. 23	12.92	11.96	1.°2	Image	*B*, *V*, *R*	VLT	Active.See Rousselot (2008)
2006 Mar. 23	12.92	11.96	1.°2	Spectrum	345–590 nm	VLT	Active.See Rousselot (2008)
2006 Mar. 30	12.91	11.92	0.°7	Image	*B*, *V*, *R*	VLT	Active.See Rousselot (2008)
2007 Mar. 24	12.23	11.30	1.°8	Image	*B*, *V*, *R*	NTT	See Rousselot (2008)
2011 Jun. 5	8.51	7.51	1.°2	Image	*B*, *V*, *R*	NOT	Active
2011 Jul. 6	8.42	7.63	4.°6	Image	*B*, *V*, *R*	NOT	Active
2011 Jul. 8	8.42	7.65	4.°7	Image	*B*, *V*, *R*	NOT	Active
2013 Jul. 4	6.59	5.57	0.°9	Image	*B*, *V*, *R*, *I*	NOT	–
2013 Jul. 5	6.58	5.57	0.°8	Image	*B*, *V*, *R*, *I*	NOT	–
2013 Jul. 6	6.58	5.57	0.°8	Image	*B*, *V*, *R*, *I*	NOT	–
2013 Jul. 7	6.58	5.57	0.°7	Image	*B*, *V*, *R*, *I*	NOT	–
2013 Jul. 8	6.58	5.56	0.°7	Image	*B*, *V*, *R*, *I*	NOT	–
2014 Apr. 28	6.06	6.13	9.°4	Image	*B*, *V*, r'	LT	–
2014 Aug. 13	5.94	4.93	1.°3	Image	*B*, *V*, r'	LT	–
2015 Jun. 2	6.02	5.55	8.°9	Image	*B*, *V*, r'	LT	–

background noise. Photometric uncertainty was computed to be equal to $(\sigma_{\rm stat}^2 + \sigma_k^2)^{1/2}$, where $\sigma_{\rm stat}$ and σ_k are, respectively, the statistical error, dominated by background uncertainty, and the scatter in the photometric transformation coefficients deduced either from the standard star images (NOT) or taken from the header description (CFHT). To evaluate $\sigma_{\rm stat}$, the SNR equation was adopted from Merline & Howell (1995). The noise model takes into account the number of pixels in the apertures used for the target and background integration as well as readout noise. Typically, $\sigma_{\rm stat}$ varied with the brightness of the target between 1 and 6 per cent, and σ_k was estimated to be less than 2 per cent. Differentiating the equation used for the $Af\rho$ calculation, we derived relative uncertainty on $Af\rho$ parameters lying between 5 and 14 per cent.

The photometric results presented in Table 4 are based on the reference aperture encapsulating the entire coma. A maximal aperture radius of 16 arcsec was used for the CFHT images obtained in 2005, which corresponded to a projected distance of 155 000 km at the target. For the images obtained in 2011, we used an aperture of 7 arcsec radius to integrate all the flux from the coma.

The $Af\rho$ parameter calculated from CFHT images, 52 000 ± 3000 cm, indicates that during the first outburst, Echeclus was among the most active Centaurs ever observed for comparable heliocentric distances (Jewitt 2009). However, the level of Echeclus' activity decreased very fast. Rousselot (2008) estimated $Af\rho$ to about 10 000 cm for 2006 March 23. During the second outburst, the $Af\rho$ parameter was calculated to be about 1200 ± 100 cm decreasing to 480 cm within approximately one month.

Photometry in the three colour bands enabled us to derive the $B - V$ and $V - R$ colour indices of dust from the images obtained in 2011. We found no change of the dust colour with a distance from Echeclus' optocentre. Colour indices derived from the June and July data sets are in agreement within the photometric accuracy, pointing out no change of the dust colour during 2011 outburst. The colour indices obtained in this study are also compatible with the colour of the innermost region of the Echeclus image estimated by Rousselot (2008) for 2006 March 23 and 30.

The $Af\rho$ values can be a proxy to estimate dust production rate, when assuming reasonable physical parameters of dust grains

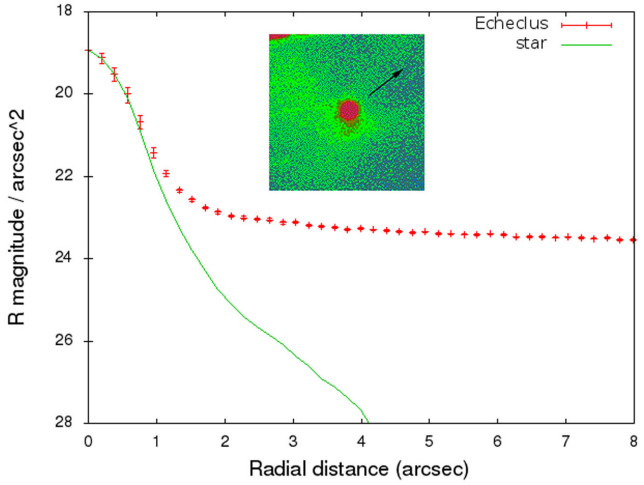

Figure 1. SBP for the second outburst constructed with the NOT observational data obtained on 2011 June 5. The small image corresponds to a size of 3 arcmin and 10 arcsec. The Sun direction is indicated by the arrow.

populating the coma. We used an approach developed by Newburn & Spinrad (1985) and Singh, de Almeida & Huebner (1992). The final equation to calculate the dust mass production rate was taken from Weiler et al. (2003):

$$Q_m = Q_{\rm N}(4\pi/3)[\int \rho_{\rm d}(a)a^3 f(a){\rm d}a]. \quad (1)$$

Here, $Q_{\rm N}$ is the dust number rate; $\rho_{\rm d}(a)$ is the density of a grain, which depends on grain radius a; $f(a)$ describes the differential particle size distribution.

The limits of integration are the minimum and maximum grain radii:

$$Q_{\rm N} = \frac{Af\rho}{2\pi^2 A_B \Phi(\alpha) \int (f(a)a^2/v(a)){\rm d}a}. \quad (2)$$

In this expression, A_B is an average geometric albedo of the ensemble of dust particles in the aperture used; $\Phi(\alpha)$ is the phase function depending on phase angle α; $v(a)$ is the ejection velocity of a particle of radius a. The lower and the upper limits on dust grain radii were put at 5 and 700 μm, respectively, according to the numerical modelling of Echeclus' dust environment (see Section 5). The particle size differential function was adopted in the form of $f(a) \sim (1 - a_0/a)^M \times (a_0/a)^N$, where a_0 is the minimum grain radius, N is a slope of the function at large values of a, parameter M locates the maximum of the distribution (Hanner 1983). We fixed M and N at 27 and 4, respectively, to provide the peak radius of about 40 μm. The expression for grain density was taken from Newburn & Spinrad (1985): $\rho_{\rm d}(a) = \rho_0 - \rho_1(a/(a + a_2))$ with $\rho_0 = 3.0$ g cm^{-3}, $\rho_1 = 2.2$ g cm^{-3} and $a_2 = 2$ μm. This gives a density of about 0.9 g cm^{-3} to particles with radii corresponding to the peak of the particle size distribution.

Geometric albedo is a crucial parameter to calculate dust production rate. We fixed average geometric albedo in a given wavelength region at 0.1 adopting a phase function in the form of $10^{-0.4\beta\alpha}$ with a phase coefficient β fixed at 0.04.

The size-dependent outflow velocities of grains were computed with equation (3) using the model parameters from Table 10. In the range of the heliocentric distances between 13.08 and 8.42 au, the velocities between 3 and 45 m s^{-1} were derived for the limiting particle sizes $r = 700$ μm and $r = 5$ μm, respectively. The calculated dust production rate is listed in Table 4.

For the data obtained in 2013 and 2014, both with the NOT and the LT, no cometary activity could be detected. Fig. 2 presents the radial profiles obtained for these observations.

The photometric analysis for the 2013 data permitted to obtain *BVRI* magnitudes. Tables 5–8 provide the computed absolute magnitudes.

4 LIGHT-CURVE CHANGES

Owing to our large set of photometric data obtained both before and after the outburst, it is possible to test the effect of the outburst, if any, in the light-curve as well as to get information about the pole orientation because of the large time span covered by our observations.

Before the outburst, from the data obtained mainly in 2003, it was possible to derive a rotation period of 26.802 ± 0.042 h if a double-peaked light-curve is assumed and a light-curve amplitude of 0.24 ± 0.06 for the *R* band (Rousselot et al. 2005). After the outburst, the photometric data obtained in 2013 have a high SNR, although they do not allow us to detect any clear brightness variation. These data correspond to a flat light-curve or to a light-curve with an amplitude inferior to about 0.1 mag. Table 9 presents the average magnitudes (*R* band) with the standard deviation for each night. The standard deviation does not exceed 0.04 mag. Fig. 3 presents an example of these data corresponding to the night 2013 July 4 to 5. No variations in the absolute magnitude can be detected in any filter.

The information provided by our photometric data set is a significant decrease in the light-curve amplitude in the period 2003–2013. These data do not permit us to get any information about a possible rotation period change because this period cannot be computed with the observations performed after the outburst. There are three possibilities for explaining the change in the light-curve amplitude: (i) a resurfacing due to the outburst, (ii) a change in the pole orientation or (iii) a pole orientation such that the change in the relative geometry Sun–Echeclus–Earth would affect the apparent light-curve amplitude observed from the Earth.

The first hypothesis would imply that the dust ejected during the main outburst would have significantly affected the surface properties, mainly albedo and that the light-curve would be mainly due to changes in the albedo at the surface.

To test this hypothesis, we combined the new photometric observational data with the pre-outburst data for the phase function.

Table 4. Magnitudes, colours, $Af\rho$ values and dust production rates derived for the periods of activity.

UT Date	Telescope	r (au)	mb	mv	mr	$B-V$	$V-R$	$R-{\rm Af}\rho$ (cm)	Dust production rate (kg s^{-1})
2005 Dec. 22	CFHT	13.08	–	–	14.39 ± 0.01	–	–	52 000 ± 3000	780
2011 Jun. 5	NOT	8.51	18.53 ± 0.03	17.70 ± 0.01	17.08 ± 0.03	0.83 ± 0.03	0.62 ± 0.03	1200 ± 100	20
2011 Jul. 6	NOT	8.42	19.75 ± 0.04	18.87 ± 0.04	18.32 ± 0.03	0.88 ± 0.06	0.55 ± 0.05	490 ± 80	10
2011 Jul. 8	NOT	8.42	19.73 ± 0.02	18.89 ± 0.02	18.36 ± 0.02	0.84 ± 0.03	0.53 ± 0.03	470 ± 30	10

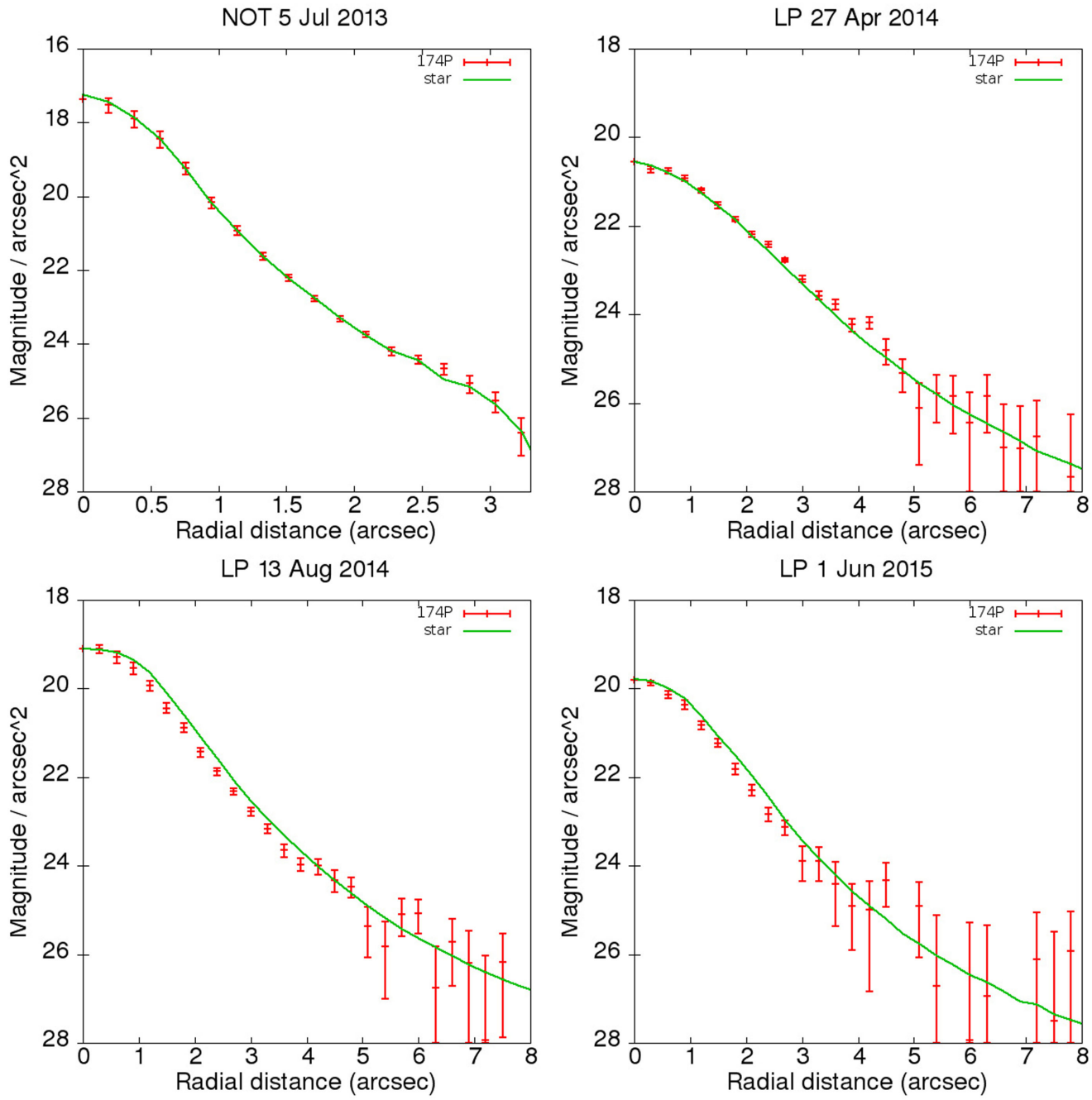

Figure 2. SBPs obtained for the 2013, 2014 and 2015 observations, performed when Echeclus was inactive. The seeing was approximately 0.8 arcsec for the NOT images, 3 arcsec for the LT on 2014 April 27 and 2 arcsec for the other LT data. No cometary activity could be detected during these observations.

Fig. 4 represents how the NOT observational data can be superimposed to the preoutburst data in this phase function. It is a copy of fig. 6 already published in Rousselot et al. (2005) with the new observational data superimposed to it. They represent a simple average of all the observations in the *R* and *v* bands with their standard deviations, for each different observing night. It can be seen that the postoutburst data fit very well the preoutburst data for the phase function. No significant change of the physical properties (including albedo) for the surface of Echeclus can consequently be detected.

Another argument to rule out this hypothesis is that the light-curve obtained with the pre-outburst data seems to be double peaked. Such a light-curve is indicative of changes due to a non-spherical shape of the nucleus rather than due to albedo changes at the surface.

The second hypothesis, a change of the pole orientation generated by the outburst, can be examined on the basis of an estimate of the mass of dust ejected relative to Echeclus' mass. The dust production rate can be estimated to about 780 kg s^{-1}, from Table 4. The duration of the event (see the next section) can be estimated to about 5 h. The total ejected mass would then be about 1.4×10^7 kg at a few tens of metres per second. Such a mass is negligible to what can be estimated for the total mass of Echeclus. With an estimated diameter of 83.6 km (Stansberry et al. 2008) and a density of about 1000 kg m^{-3}, we can estimate Echeclus' mass to be

Table 5. Absolute magnitudes measured for Echeclus for the *B* band. The MJD is corrected for the light travel time. This is only a sample table, the full table is available online.

MJD	Mag.
56477.0791	10.741 ± 0.047
56477.0862	10.758 ± 0.043
56477.0928	10.746 ± 0.041
56477.1007	10.694 ± 0.006
56477.1083	10.747 ± 0.040
56477.1150	10.715 ± 0.006
56477.1228	10.731 ± 0.047
56477.1301	10.777 ± 0.011
56477.1591	10.723 ± 0.040
56477.1659	10.821 ± 0.076

Table 6. Absolute magnitudes measured for Echeclus for the *v* band. The MJD is corrected for the light travel time. This is only a sample table, the full table is available online.

MJD	Mag.
56477.0814	9.849 ± 0.016
56477.0880	9.853 ± 0.035
56477.0958	9.844 ± 0.019
56477.1030	9.857 ± 0.012
56477.1108	9.854 ± 0.019
56477.1180	9.892 ± 0.016
56477.1251	9.834 ± 0.022
56477.1317	9.854 ± 0.018
56477.1615	9.888 ± 0.009
56477.1678	9.827 ± 0.015

Table 7. Absolute magnitudes measured for Echeclus for the *R* band. The MJD is corrected for the light travel time. This is only a sample table, the full table is available online.

MJD	Mag.
56477.0799	9.297 ± 0.036
56477.0823	9.321 ± 0.028
56477.0855	9.290 ± 0.029
56477.0876	9.320 ± 0.035
56477.0898	9.345 ± 0.032
56477.0920	9.313 ± 0.035
56477.0949	9.330 ± 0.009
56477.0973	9.348 ± 0.007
56477.0993	9.312 ± 0.027
56477.1015	9.331 ± 0.025

$\sim 3.0 \times 10^{14}$ kg. Even with a longer duration of the event at the origin of the outburst (a few weeks), the total ejected mass would still be negligible compared to Echeclus' mass. The hypothesis of a change in the pole orientation can, consequently, be ruled out.

The third hypothesis, i.e. that the change in the light-curve amplitude would come from the relative geometry with respect to the Earth seems more realistic than the two first ones. Fig. 5 represents the orbit of Echeclus with its position for the different epochs of observations. It can be seen that there is a large fraction of the orbit covered between the first and last photometric observations. So there is an important change in the relative geometry of the line of sight with respect to the Earth.

Table 8. Absolute magnitudes measured for Echeclus for the *I* band. The MJD is corrected for the light travel time. This is only a sample table, the full table is available online.

MJD	Mag.
56477.0838	8.863 ± 0.014
56477.0907	8.827 ± 0.021
56477.0978	8.880 ± 0.028
56477.1056	8.846 ± 0.028
56477.1123	8.859 ± 0.010
56477.1199	8.863 ± 0.024
56477.1277	8.881 ± 0.026
56477.1341	8.851 ± 0.031
56477.1640	8.910 ± 0.025
56477.1710	8.853 ± 0.028

Table 9. Average absolute magnitudes (*R* band) and standard deviations for NOT data.

Date	Average mag.	Standard deviation
2013 Jul. 4	9.341	0.025
2013 Jul. 5	9.288	0.022
2013 Jul. 6	9.325	0.019
2013 Jul. 7	9.333	0.030
2013 Jul. 8	9.318	0.041

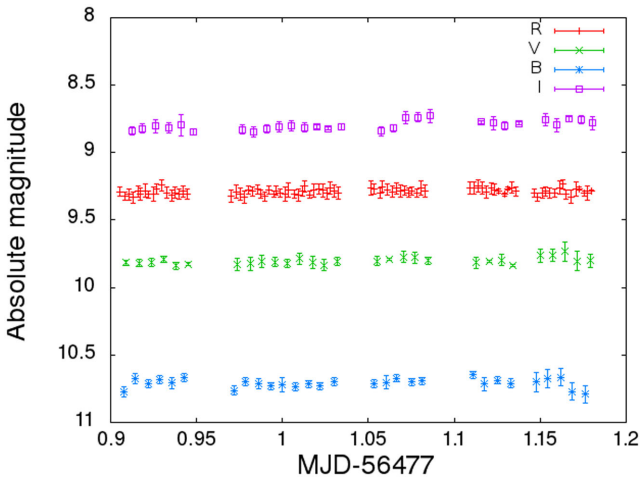

Figure 3. Example of photometric data obtained during the night 2013 July 4–5 with the 2.5-m NOT. No variations can be detected above about 0.1 mag.

A flat light-curve in 2013 July implies that the pole axis was at that time, more or less, pointing to the Earth. Conversely, a significant light-curve amplitude in 2003 April implies that the pole axis at that time was, more or less, perpendicular to the Sun/Earth direction. The first constrain implies that the obliquity is probably high, i.e. that the rotation axis has a small angle with respect to the ecliptic plane. Because of the probable double-peak nature of the light-curve its amplitude is probably mostly due to the elongated shape of Echeclus. With a light-curve amplitude equal to 0.24 (*R* band), a lower limit for the axis ratio a/b where a and b are the semiaxes such as $a \geq b$ is $a/b \geq 1.25$ (Rousselot et al. 2005).

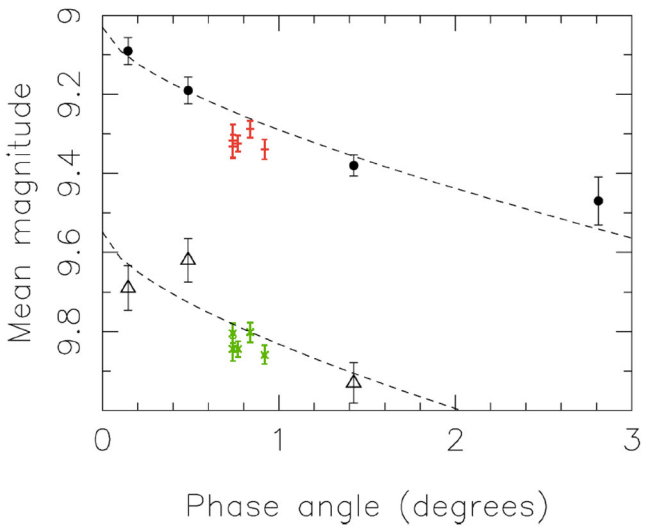

Figure 4. Phase function of Echeclus as it was measured before the outburst with the new observational data obtained in 2013 superimposed on fig. 6 of Rousselot et al. (2005): filled circles are for the *R* band and triangles for the *v* band. The red and green points with error bars at phase angle $\sim 0\overset{\circ}{.}9$ are the data obtained in this work for the *R* band and *v* band, respectively. Each point corresponds to the average of the different observing nights with the error bars corresponding to 1σ. The dashed lines correspond to the H–G scattering parametrization computed with the preoutbursts data.

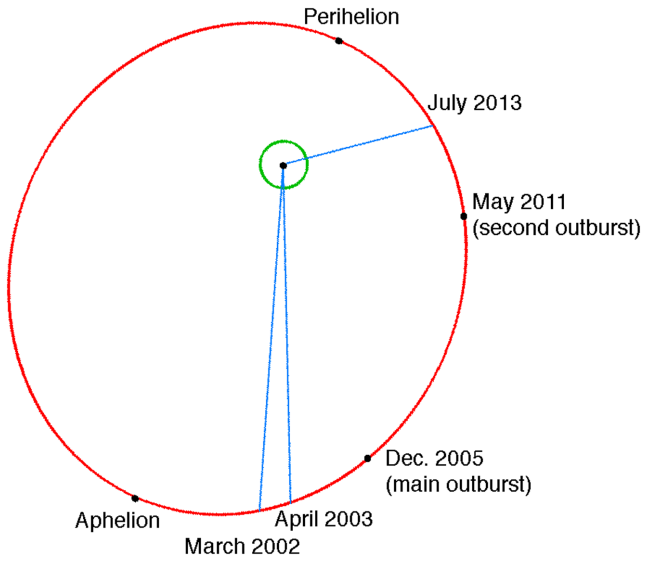

Figure 5. Orbit of Echeclus (red) and the Earth (green) with the position of Echeclus for the different epochs corresponding to photometric data.

It would be possible to test if the light-curve change is due to a geometric effect by measuring again this light-curve soon, i.e. around 2016–2017. Echeclus has now passed its perihelion and is roughly at the opposite on its orbit compared to 2003, or perpendicular to its position in 2013 (see Fig. 5). We would expect, consequently, a light-curve amplitude roughly equal to the one measured during our 2002–2003 observations, if the light-curve change observed is due to a geometric effect. On the contrary, some resurfacing process would likely be at the origin of the light-curve change observed.

5 MODELING OF THE OUTBURST

Our observational data also allow us to model the main outburst itself, i.e. how the dust has been ejected from the nucleus. Because the morphology of the coma was rather complex, it is not a simple task. So far no acceptable explanation of the possible active processes that occurred on the surface of the nucleus was proposed (Bauer et al. 2008; Rousselot 2008). For modelling the main outburst, we tried to reconstruct the observed appearance by using a Monte Carlo technique. We used the model already developed to fit the dust environment of distant comets (Korsun et al. 2010).

Any modelling of the active processes responsible of the outburst must be able to explain the following observational facts mentioned by Weissman et al. (2006), Bauer et al. (2008) and Rousselot (2008).

(i) The duration of the outburst was confined to the period within the 12 months spanning 2005 December – 2006 December.

(ii) The maximum of activity, detected on 2005 December 22, is very important ($Af\rho = 52\,000$ cm). It corresponds to a dust production rate of a few hundreds of kilograms per second, of the order of 30 times that seen in other Centaurs.

(iii) The morphology of the coma is strongly anisotropic with a distinct source of activity of Echeclus itself. This source was located at about 7 arcsec of the nucleus (corresponding to a projected distance of 65 000 km at the comet) in February–March. This distance decreases in 2006 May up to only 2.7 arcsec.

Fig. 6 presents an image obtained by the VLT+FORS 1 on 2006 March 23 (*R* filter). It shows a general overview of the coma pattern.

From these observational facts, we first conclude that the morphology of the observed coma cannot be explained by an isotropic outflow. Several local distinct active zones were most likely activated on the surface of the nucleus. The brightest feature cannot be explained by an ejected fragment as there is no point-like feature within it (Rousselot 2008). It is likely the result of a short lasting process.

The widespread feature appearing towards the Sun was formed by some dust ejected from the nucleus earlier than those that formed the bright feature towards the tail. The lack of a clearly defined maximum of brightness in this feature in the vicinity of the nucleus indicates that this active process, at least, greatly declined before the observations. Furthermore, the orientation of this detail can be determined by the inclination of the rotation axis of the nucleus. A rotation period of 26.8 h was derived from the analyses of the light-curve of Echeclus when it was inactive (Rousselot et al. 2005). Bauer et al. (2008) estimated the maximum size of the ejected particles to 700 μm, within an order of magnitude, for Echeclus. For modelling the main outburst, we used our experience in fitting the dust environment of the distant comets (Korsun & Chörny 2003; Korsun et al. 2010; Rousselot et al. 2014).

Our model runs concretized a possible scenario of the formation of the observed coma. The observational data can be fitted with a highly inclined spin axis of the nucleus with respect to the normal of the orbital plane. We fixed our model runs with an inclination of 70° towards the ξ-axis direction and 40° towards the η-axis direction within the cometocentric reference frame (see Fig. 8). In this case, the north pole of the nucleus is much more illuminated by the solar radiation than the Southern hemisphere. The brightest spot towards the tail can be reproduced if it is assumed that two active short lasting events happened prior to the observations. The events were activated approximately at the same time, but with significantly different location on the nucleus. The results of our final model run indicated that one active zone was located at the southern latitude of −15°

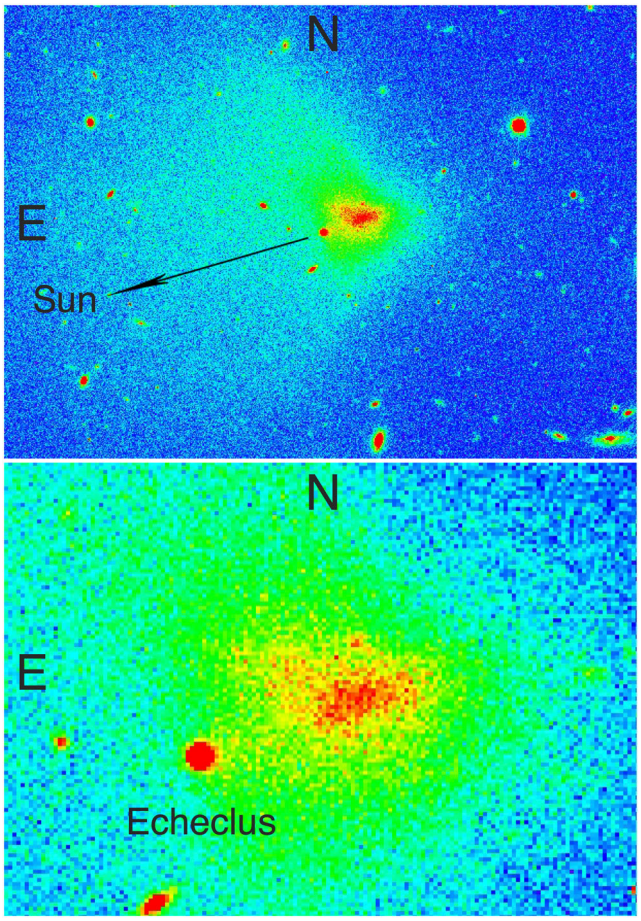

Figure 6. Image of Echeclus with the combination VLT+FORS 1 on 2006 March 23 (*R* band). Top: the scale is 2 arcmin from left to right. Bottom: close-up view of top image with a smaller scale (30 arcsec from left to right).

(source 1), while the other one was located at the northern latitude of 30° (source 2). There is a correlation between the longitudes of the active zones and the time intervals between the beginning of activity of the two active zones. We can accept a difference in longitude of 105° – or 7.8 h in time interval – between the events, intermediate values provide also valuable results.

Fitting the sunward widespread feature was more difficult. There is no clearly pronounced photometric maximum near the nucleus and a first attempt was done by considering a short lasting event like the ones considered above. Unfortunately, this attempt failed to reproduce the observational data. In a second attempt, we considered a scenario for the active process similar to the one considered for comet 29P/Schwassmann–Wachmann 1 (e.g. Trigo-Rodríguez et al. 2008), i.e. a sharp increase of the brightness followed by a gradual decrease lasting one or several months. We tried to fit the dust production of the active zone by assuming a power law with a power index of −2, as the most suitable for this case. We located this active zone in the Northern hemisphere at the latitude of 40° (source 3) and considered it almost uncollimated. We described the outflow of the matter from this zone within a cone with a half open angle of 80°. An acceptable day/night ratio activity was ∼1, which means that the level of the jet activity was more or less the same for the night side of the nucleus with respect to the day side.

Ejection velocities of dust, v_d, were scaled by

$$v_d = (A_0 + B_0\sqrt{a})^{-1} r^{-0.5}, \quad (3)$$

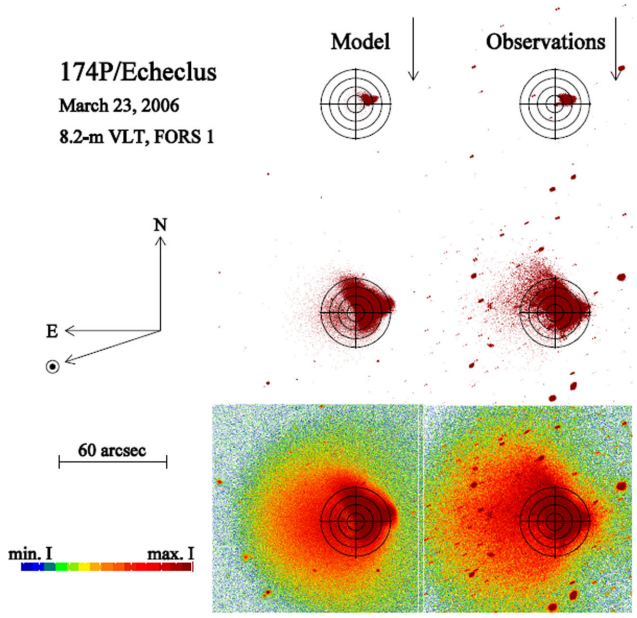

Figure 7. Modelled and observed appearance of Echeclus on 2006 March 23. A superimposed radially spacing grid is introduced for a better perception of the results. The two upper sections represent the cuts of our results at higher intensity levels for showing the inner coma. The scale bar of 60 arcsec, directions to north, east and the Sun are marked to the left. The colour bar represents scaling of the intensity levels.

where A_0 and B_0 are model parameters, factor $r^{-0.5}$ represents the heliocentric distance dependence of the velocities (Sekanina et al. 1992). The velocities were not the same for the different sources of dust and an acceptable result was obtained with v_d (source 1):v_d (source 2):v_d (source 3) = 1.0:1.5:2.3 ratio.

We converged to the final model when we managed to reproduce the main morphological details of the observational data obtained in 2006 March. The result is shown in Fig. 7, and a complete set of the parameters is listed in Table 10 (see Fig. 8 for the definition of the ξ- and η-axis).

In order to test our modelling of the observational data obtained in 2006 March, we considered the CFHT archive data obtained on 2005 December 22. These data are the first one available after the outburst, before the official discovery by Choi et al. (2006b). This test was very sensitive to the escape velocities and to the timing considered to the different active processes. For modelling these archive data, we used the same model parameters listed in Table 10. The result is shown in Fig. 9.

The conclusion of our modelling is that we can summarize the activity of Echeclus as follows. We can explain the appearance of the coma if we assume that two short lasting events producing the activity occurred on the surface of Echeclus within a short time interval (of the order of a few hours) around 2015 December 7. Since the duration of the processes was about a few hours, there were no ejections from these zones at the moments of observation (2005 December 22 and, a fortiori, 2006 March 23), the remnant clouds of dust particles that originated from these sources were only detected later. The non-collimated outflow started somewhat earlier, around 2005 November 15. It evolved from a sharp increase of activity followed by a gradually decreasing dust production rate. It was almost inactive on 2006 March 23, while still important on 2005 December 22, but with a much lower level comparing to its initial level.

Table 10. Summarized model parameters used for our dust environment modelling. For the activity durations the FWHM corresponds to the time span between the brightness distribution at half-maximum, which was caused by the active event.

Parameter	Source 1	Source 2	Source 3
Spin axis inclination		70° towards the ξ-axis and 40° towards the η-axis direction	
Start activity	2005 December 7	2005 December 7	2005 November 15
Source longitude	0°	105°	–
Source latitude	−15°	30°	40°
Activity durations	FWHM = 1.5 h	FWHM = 5.0 h	Power-law index = −2
Collimation	Cone, half-angle = 8°	Cone, half-angle = 25°	Uncollimated
'day/night' activity	–	–	1
Solid sizes	5–100 μm	5–100 μm	5–700 μm
Power index, a^x, x =	−3.5	−4.0	−4.0
B_0 (equation 3), $A_0 = 0$	0.0053	0.0035	0.0023
Velocities (a = 5 μm, r = 12.92 au)	23.5 m s^{-1}	35.2 m s^{-1}	54.0 m s^{-1}

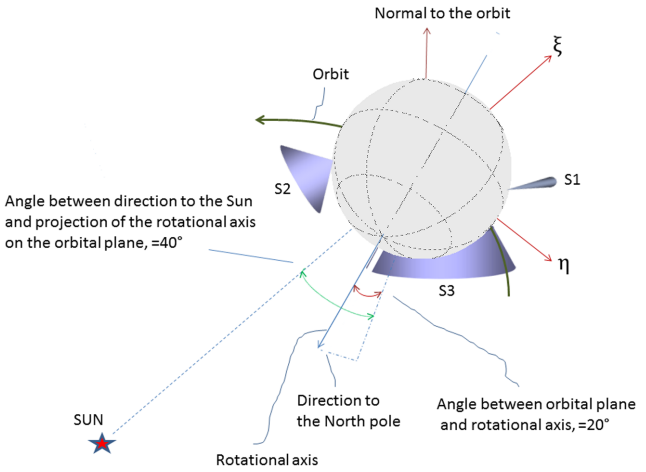

Figure 8. Representation of the ξ- and η-axis with respect to Echeclus.

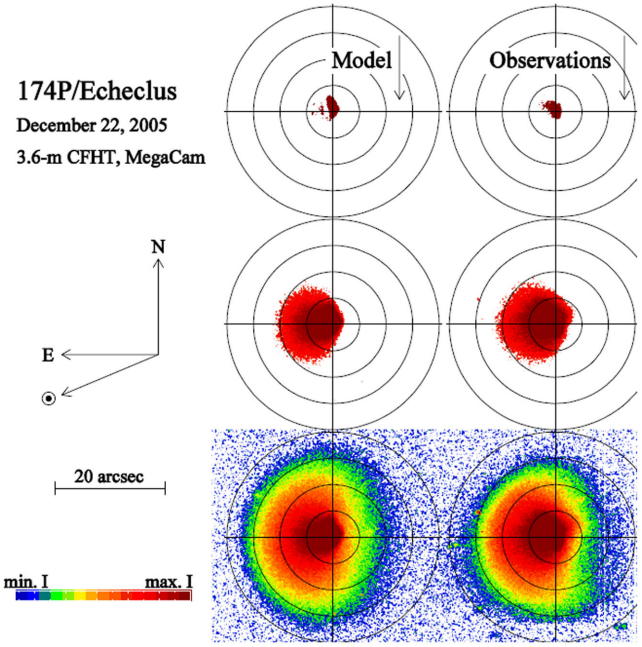

Figure 9. Modelled and observed appearance of Echeclus on 2005 December 22. A superimposed radially spacing grid with the same scale as in Fig. 7 is introduced for a better perception of the results. The two upper sections represent the cuts of our results at higher intensity levels for showing the inner coma. The scale bar of 20 arcsec, directions to north, east and the Sun are marked to the left. The colour bar represents scaling of the intensity levels.

The model findings are robust for a spherically symmetric nucleus with outflows normal to the surface. The shape of Echeclus' nucleus is likely not an ideal sphere and outflows into jets are normal to the local surface as it was observed for comet 67P/Churyumov–Gerasimenko (Lin et al. 2015). If so, the activity of the three active zones remotely located on the nucleus surface could likely be reduced to the activity of one compact zone with the outflow space orientations determined for the spherical nucleus. In this case, all our model parameters are correct with the exception of the locations of the active zones defined by their longitudes and latitudes. Most likely, the location of the single active area would be close to that determined for the uncollimated Source 3.

The pole orientation provided by our modelling in this section corresponds also to a large obliquity, as it was inferred from the light-curve change. The angle between the direction to the Sun and the projection of the rotational axis on the orbital plane (40°, see Fig. 8) does not correspond to a pole axis oriented – more or less – to the Sun direction in 2013 July (see Fig. 5). This value of 40° is probably underestimated and related to the limitation of our modelling, which considers that Echeclus has a spherical shape and is not elongated (the true elongation being probably, at least, 1.25, see above).

6 DISCUSSION

In 2005, Echeclus sustained an outburst that lasted several months, with an apparent source that appeared as if it moved away from the nucleus. Weissman et al. (2006) suggested that this 'secondary' source could not have been a large fragment ejected from the primary or an impact because the activity was not comparable to the one sustained by comet 9P/Tempel 1 after the Deep Impact experiment. Bauer et al. (2008) considered that the grain size distribution in the coma was consistent with a steady cometary activity, as observed for example by the Stardust spacecraft on comet 81P/Wild 2, and not consistent with an impact-driven activity such as observed

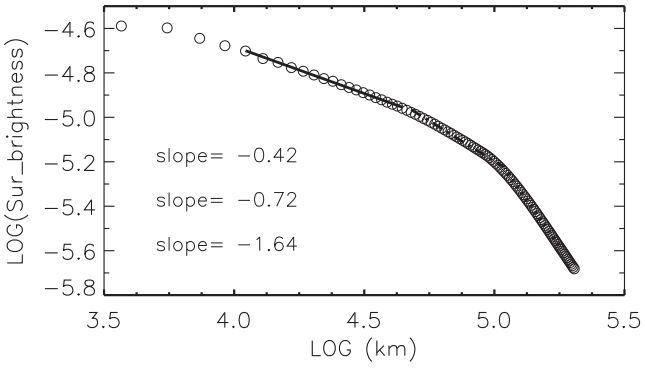

Figure 10. SBP computed from the CFHT images obtained on 2005 December 22. Three different slopes are clearly visible and the corresponding values are written in the graph.

by the Deep Impact spacecraft. In this work, we show that, in contrast to Bauer et al. (2008) who derived an activity generated by a steady-state, isotropic or nearly isotropic outflow, the structure observed in Echeclus' coma could be reproduced by localized sources on the surface. In 2011, Echeclus sustained a second outburst.

A key point in our modelling is the ejection velocity, which is significantly smaller than the one considered by Bauer et al. (2008). These authors found a minimum dust ejection velocities of the order of 200 m s^{-1}, in contrast to the values varying from 23.5 to 54 m s^{-1} used in our modelling of the main outburst. Such values can be compared to other works dedicated to outbursts observed at large heliocentric distances, which correspond to all smaller values.

(i) West, Hainaut & Smette (1991) observed an outburst in Halley's comet at 14.3 au and derived, from images taken during a two month period, an expansion velocity of 14.5 m s^{-1}.

(ii) Kidger et al. (1996) analysed the growth of the linear section of the jet in comet Hale–Bopp, when it was at large heliocentric distances, and computed a projected expansion velocity of 32 m s^{-1}.

(iii) Fulle (1992) fitted the dust coma of comet P/Schwassmann–Wachmann 1 at $r \sim 6$ au by using a Monte Carlo model with ejection velocities of about 10–20 m s^{-1} (see their fig. 2).

(iv) Fulle, Cremonese & Böhm (1998) fitted the dust coma of comet Hale–Bopp at $r \sim 13$ au by using a Monte Carlo model with ejection velocities of about 80–100 m s^{-1} (see their fig. 2 for values corresponding to 1500 d before perihelion).

Another interesting test to know if a cometary coma is in steady state consists in computing its SBP. In a log–log graph and a canonical coma in a steady state with surface brightness proportional to $1/\rho$, the slope of the SBP must be close to -1. Fig. 10 presents the SBP computed for the CFHT data, obtained on 2005 December 22. From this figure, it can be seen that the SBP presents three different slopes corresponding to different ranges of cometocentric distances: (i) below a few thousands of kilometres (slope $= -0.42$), (ii) between a few thousands and about 100 000 km (slope $= -0.72$) and (iii) beyond ∼100 000 km (slope $= -1.64$).

The last region (slope steeper than 1.5) probably corresponds to the effect of radiation pressure that become important for large cometocentric distances. The intermediate region is likely the region where a secondary source of grains exists (possible fragmentation).

Possible origins for Echeclus' cometary activity include impacts and fragmentation, which were ruled out based on the observations of the first outburst. We are thus considering here internal processes as possible causes for the observed activity pattern. Huebner et al. (2006) described the possible origins of outbursts, related to both sublimation of ices and transition between amorphous and crystalline water ice. Both phase transitions may be accompanied by the build-up of internal pressure if the porous structure of cometary material is sealed, for example due to the presence of a compacted dust mantle at the surface. With gas accumulating underneath the surface, large stresses would be created and may results in an explosion-like outburst of gas. Sublimation of volatiles is however limited to very volatile species at the distance Echeclus' outbursts were observed (around 13 and 8 au).

Crystallization of amorphous ice on Centaurs was studied by Guilbert-Lepoutre (2012), on which we base the following discussion. The current orbit of Echeclus is equivalent in terms of energy received from the Sun to a circular orbit at about 8.5 au. Being nearly pole-on, Echeclus falls in the top-right corner of fig. 5 of Guilbert-Lepoutre (2012) describing the depth reached by the crystallization front after 10^5 years in the giant planet region. In the case of Echeclus, we might expect the transition between amorphous and crystalline water ice to have reached up to 50 m. Although this front remains relatively close to the surface, the process in itself would not be expected to contribute to Echelus' activity after such a timescale, unless a recent change in orbit modified the surface energy balance. Alternatively, an impact could have triggered the local removal of crystallized material. We stress again that this possibility was ruled out for the first outburst in 2005, and indeed we can further argue against an impact-induced outburst, since crystallization of recently exposed amorphous water ice at 13 au where the equilibrium temperature is around 77 K would occur in orders of magnitude more time than needed to produce the outburst observed in 2005.

However, the 2005 event must have induced changes for the nucleus. Bauer et al. (2008) inferred that the mass loss of Echeclus during this event exceeded all estimates made for other Centaurs and Jupiter Family Comets. We can easily imagine that large chunks of material were locally removed by erosion for example, since fragmentation was deemed unlikely, so that the subsequent localized crystallization of freshly exposed amorphous ice could possibly explain the second outburst. However, the transition time-scale at 8 au is of the order of 1000 years, so it is unlikely that crystallization was indeed responsible for any of the two observed outbursts. We are left with no possible internal process as a plausible origin for the observed outbursts, unless we assume that the internal structure of Echeclus is heterogeneous.

Indeed, Rosenberg & Prialnik (2010) studied the effect of internal inhomogeneities on the activity of comets, and 67P/Churyumov–Gerasimenko in particular. They showed that such features could actually be detected in the activity pattern of a comet, where erratic behaviours are induced by many 'patches' with different thermophysical properties randomly distributed inside the nucleus. They showed that outbursts may arise at any moment of the orbit, even at large heliocentric distances, with production rates that can exceed those expected at perihelion. These outbursts were found to have diverse intensities and durations, typically days to weeks. The erratic outbursty behaviour of Echeclus may be the result of intrinsic internal inhomogeneities, without any special process needed to explain it.

7 CONCLUSION

Echeclus is the Centaur that presented, so far, the largest outburst ever detected since these planetary bodies are known ($Af\rho$ larger than about 5×10^4 cm). Since its discovery in 2000, this object

experienced three outburts. A first and main one at the end of 2005 and two smaller ones in 2011 May and 2016 August.

From the observational data presented in this paper, we conclude the following.

(i) The light-curve amplitude strongly decreases between 2003 and 2013. This change is certainly related to a geometric effect, i.e. a rotation axis strongly inclined with respect to the normal of the orbital plane.

(ii) The main outburst corresponds to different events that occurred between about 2005 November 15 and December 7. A satisfactory fit of the observational data can be obtained with two short events (sources 1 and 2) lasting a few hours and a longer one happening before (source 3). Our fit also suggests a high obliquity for the rotation axis.

(iii) The most probable explanation is related to internal inhomogeneities of the nucleus.

(iv) No changes in the dust colour indices could be detected both inside the coma and between the two first outbursts. Their size distribution was, consequently, probably more or less the same for these two events.

Because of the unpredictable aspect of the outbursts detected so far in Echeclus and the changes also observed in the light-curve amplitude, this object constitutes an important target for a photometric monitoring in the coming years. This photometric monitoring could permit to test if the observed change in the light-curve is really due to a geometric effect. It could also help to detect other outbursts, such as the one detected after the perihelion passage, on 2016 August 28.

ACKNOWLEDGEMENTS

The research leading to these results has received funding from the European Community's Seventh Framework Programme (FP7/2013-2016) under grant agreement number 312430 (OPTICON). This work is based on observations made with the Nordic Optical Telescope and the Liverpool Telescope at the Spanish Observatorio del Roque de los Muchachos of the Instituto de Astrofisica de Canarias.

REFERENCES

A'Hearn M. F., Schleicher D. G., Millis R. L., Feldman P. D., Thompson D. T., 1984, AJ, 89, 579
Bauer J. M., Choi Y.-J., Weissman P. R., Stansberry J. A., Fernández Y. R., Roe H. G., Buratti B. J., Sung H.-I., 2008, PASP, 120, 393
Choi Y., Weissmann P. R., Chesley S., Bauer J., 2006a, Cent. Bur. Electron. Telegrams, 563
Choi Y., Weissmann P. R., Polishook D., 2006b, IAU Circ., 8656
Fulle M., 1992, Nature, 359, 42
Fulle M., Cremonese G., Böhm C., 1998, AJ, 116, 1470
Gladman B., Marsden B. G., Vanlaerhoven C., 2008, in Barucci M. A., Boehnhardt H., Cruikshank D. P., Morbidelli A., Dotson R., eds, The Solar System Beyond Neptune. Univ. Arizona Press, Tucson, p. 43
Guilbert-Lepoutre A., 2012, AJ, 144, 97
Hanner M. S., 1983, in Gombosi T. I., ed., Cometary Exploration, Vol. 2. Hungarian Acad. Sci., Budapest, p. 1
Horner J., Evans N. W., Bailey M. E., 2004, MNRAS, 354, 798
Huebner W. F., Benkhoff J., Capria M.-T., Coradini A., De Sanctis C., Orosei R., Prialnik D., eds, 2006, Heat and Gas Diffusion in Comet Nuclei. ESA, Noordwijk
Jaeger M., Prosperi E., Vollmann W., Sato H., Sostero G., Guido E., 2011, IAU Circ., 9213, 2
Jewitt D., 2009, AJ, 137, 4296
Jewitt D. C., Meech K. J., 1987, ApJ, 317, 992
Kidger M. R., Serra-Ricart M., Bellot Rubio L. R., Casas R., 1996, ApJ, 461, L119
Korsun P. P., Chörny G. F., 2003, A&A, 410, 1029
Korsun P. P., Kulyk I. V., Ivanova O. V., Afanasiev V. L., Kugel F., Rinner C., Ivashchenko Y. M., 2010, Icarus, 210, 916
Kowal C. T., Liller W., Chaisson L. J., 1977, IAU Circ., 3147
Landolt A. U., 1992, AJ, 104, 340
Lin Z.-Y. et al., 2015, A&A, 583, A11
Lorin O., Rousselot P., 2007, MNRAS, 376, 881
Lowry S. C., Fitzsimmons A., 2005, MNRAS, 358, 641
Marsden B. G., 2000, MPEC Circ. MPEC 2000-Q21
Meech K. J., Belton M. J. S., 1989, IAU Circ., 4770
Merline W. J., Howell S. B., 1995, Exp. Astron., 6, 163
Newburn R. L., Spinrad H., 1985, AJ, 90, 2591
Rosenberg E. D., Prialnik D., 2010, Icarus, 209, 753
Rousselot P., 2008, A&A, 480, 543
Rousselot P., Petit J.-M., Poulet F., Sergeev A., 2005, Icarus, 176, 478
Rousselot P., Korsun P. P., Kulyk I. V., Afanasiev V. L., Ivanova O. V., Sergeev A. V., Velichko S. F., 2014, A&A, 571, A73
Sekanina Z., Larson S. M., Hainaut O., Smette A., West R. M., 1992, A&A, 263, 367
Singh P. D., de Almeida A. A., Huebner W. F., 1992, AJ, 104, 848
Stansberry J., Grundy W., Brown M., Cruikshank D., Spencer J., Trilling D., Margot J.-L., 2008, in Barucci M. A., Boehnhardt H., Cruikshank D. P., Morbidelli A., Dotson R., eds, The Solar System Beyond Neptune. Univ. Arizona Press, Tucson, p. 161.
Tholen D. J., Hartmann W. K., Cruikshank D. P., Lilly S., Bowell E., Hewitt A., 1988, IAU Circ., 4554, 2
Trigo-Rodríguez J. M., García-Melendo E., Davidsson B. J. R., Sánchez A., Rodríguez D., Lacruz J., de Los Reyes J. A., Pastor S., 2008, A&A, 485, 599
Weiler M., Rauer H., Knollenberg J., Jorda L., Helbert J., 2003, A&A, 403, 313
Weissman P. R., Chesley S. R., Choi Y. J., Bauer J. M., Tegler S. C., Romanishin W. J., Consolmagno G., Stansberry J. A., 2006, in AAS/Division for Planetary Sciences Meeting Abstracts vol. 38. p. 551
West R. M., Hainaut O., Smette A., 1991, A&A, 246, L77

SUPPORTING INFORMATION

Supplementary data are available at *MNRAS* online.

Table 5. Absolute magnitudes measured for Echeclus for the *B* band.
Table 6. Absolute magnitudes measured for Echeclus for the *v* band.
Table 7. Absolute magnitudes measured for Echeclus for the *R* band.
Table 8. Absolute magnitudes measured for Echeclus for the *I* band.

Please note: Oxford University Press is not responsible for the content or functionality of any supporting materials supplied by the authors. Any queries (other than missing material) should be directed to the corresponding author for the article.

This paper has been typeset from a TEX/LATEX file prepared by the author.